CrystEngComm

PAPER

View Article Online
View Journal | View Issue

Halogen···halogen *contra* C–H···halogen interactions†

Marcin Podsiadło, Anna Olejniczak and Andrzej Katrusiak*

Cite this: *CrystEngComm*, 2014, **16**, 8279

Received 31st January 2014,
Accepted 5th June 2014

DOI: 10.1039/c4ce00241e

www.rsc.org/crystengcomm

Pressure affects the competition between C–H···X hydrogen bonds and X···X halogen···halogen interactions. In bromomethane, CH_3Br, pressure changes the molecular arrangement of the two solid-state phases of this compound: low-pressure phase α is dominated by halogen···halogen interactions, whereas above 1.5 GPa the β phase is governed by C–H···halogen bonds. The CH_3Br phase α is isostructural with solid CH_3I of orthorhombic space group *Pnma*, while CH_3Br phase β is polar, isostructural with CH_3Cl and CH_3CN crystals, of orthorhombic space group $Cmc2_1$. The crystal structures of CH_3Cl (b.p. = 249.1 K) and CH_3Br (b.p. = 276.7 K) have been determined by high pressure single-crystal X-ray diffraction up to 4.38 GPa and 2.85 GPa, respectively. In CH_3Br, pressure of 1.5 GPa enforces the close packing and opposite electrostatic-potential matching between molecular surfaces in contact. The interweaved C–H···X bonded diamondoid networks of β-CH_3X are similar to those of acetonitrile, H_2O ice VII and solidified X_2 halogens. The phase diagrams of CH_3Br and CH_3Cl have been constructed.

Introduction

The molecular arrangement in crystals is most often associated either with Kitaigorodski's close packing rule or with specific intermolecular interactions, such as OH···O hydrogen bonds in H_2O ice. Even weak specific interactions, such as halogen···halogen,[1,2] halogen···O[3–5] and CH···O contacts,[6] can compete between themselves[7,8] and with the close packing rule.[9] Members of the group of halomethanes (CH_3X, X = Cl, Br, I) are the simplest organic polar compounds and ideal models for studying weak halogen···halogen and C–H···halogen interactions. In many molecular crystals without strong hydrogen bonds the X···X and C–H···X interactions dominate the molecular arrangement and are the shortest intermolecular contacts in the crystal structure.[10] Pressure can considerably modify the intermolecular interactions in crystals. It was evidenced that weak hydrogen bonds CH···O[11–13] and CH···N[14] significantly increase their role in high-pressure structures. For example, formamide[15] and (+)-sucrose[16] transform at high pressure as a result of the increased role of CH···O interactions, in sucrose competing with OH···O bonds. The competition between halogen···halogen and C–H···halogen interactions was studied for a series of six dihalomethanes CH_2XY (X, Y = Cl, Br, I). They crystallize in several structural types of space group *Pbcn* (CH_2Cl_2, CH_2BrCl phase II), *C*2/*c* (CH_2Br_2, CH_2I_2 phase I, CH_2BrCl phase I, CH_2BrI), *Pnma* (CH_2ClI phase III), $Pna2_1$ (CH_2ClI phase IV) and *Fmm*2 (CH_2I_2 phase II).[17–22] In all of these compounds and their polymorphs, halogen···halogen interactions persist despite considerable structural differences. However, the persistence of halogen···halogen contacts in dihalomethanes can be due to the geometric effect of at least two-thirds of the molecular surface (for CH_2Cl_2) belonging to the halogen atoms. In these structures, even if other contacts are preferred and formed, the halogen···halogen contacts would be formed simply for there is no other molecular surface available. In methyl halides, of general formula CH_3X, there is one halogen atom per molecule (hence its molecular surface is smaller than those of CH_2X_2 and $CHCl_3$) and the competition between C–H···X and X···X interactions is more apparent. Therefore we have studied the structures of methyl halides in order to determine the effect of pressure on X···X and H···X interactions. CH_3Cl and CH_3Br are gases under normal conditions, which required that a special technique be developed and employed for loading these gases into the diamond-anvil cell (DAC).

The low-temperature/ambient-pressure CH_3Br and CH_3I crystals are isostructural, of the orthorhombic space group *Pnma*,[23,24] while the CH_3Cl crystal has a different structure, of the orthorhombic space group $Cmc2_1$.[25] At room temperature the *Pnma*-symmetric CH_3I structure is stable up to at least 2.5 GPa.[26] No polymorphs or phase transitions were detected in CH_3Cl and CH_3I at low temperature, while calorimetric measurements indicated that CH_3Br undergoes a first-order phase transition at 173.75 K.[27] The Raman and far infrared spectra showed that the deuterated analogue, CD_3Br, transforms at 158 K, about 16 K below the transition of CH_3Br.[28] The crystal structures of CD_3Br in both its phases were determined by neutron powder diffraction at 175 K and 146 K.[29] We have

Faculty of Chemistry, Adam Mickiewicz University, Umultowska 89b, 61-614 Poznań, Poland. E-mail: katran@amu.edu.pl; Fax: +48 61 8291555; Tel: +48 61 8291590

† Electronic supplementary information (ESI) available: Detailed experiment and structure description. CCDC 957707–957715. For ESI and crystallographic data in CIF or other electronic format see DOI: 10.1039/c4ce00241e

presently established that in that study the high- and low-temperature phases were confused. Initially, the sample had been kinetically flash-frozen and cryo-ground in the temperature and atmosphere of liquid nitrogen. In accordance with Ostwald's rule the sample crystallized in the high-temperature phase α and at 146 K it was metastable throughout data collection. This α-phase determined at 146 K was of the orthorhombic space group *Pnma*. Then the sample had transformed to the low-temperature β phase before it was warmed to 175 K, *i.e.* 17 K above the transition temperature of CD_3Br at 158 K. Again, the β phase remained metastable under these conditions for the duration of powder data collection at least. Thus incidently at higher temperature the crystal structure of low-temperature phase β was determined. This β-phase is of the orthorhombic space group $Cmc2_1$. Consequently, in that previous study the persistence of crystal phases in their metastable regions caused the reversed assignment of high- and low-temperature phases α and β, respectively.[29]

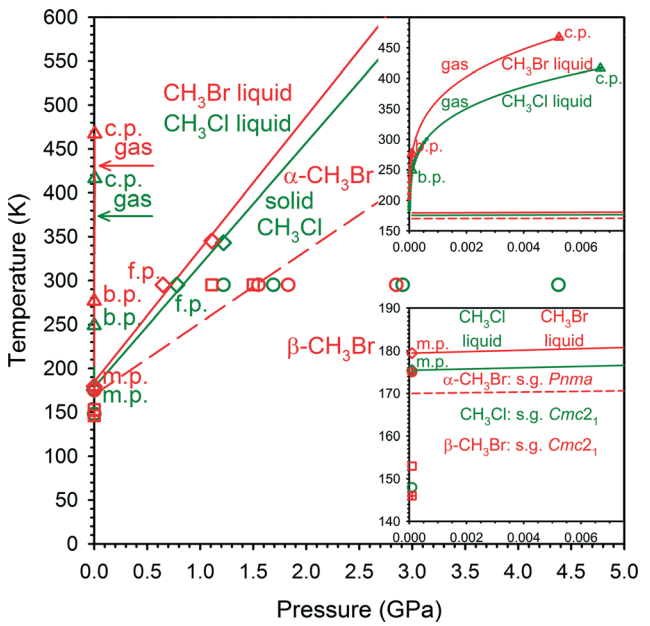

Fig. 1 Phase diagrams of CH_3Cl (green) and CH_3Br (red) superimposed for convenient comparison (they are shown separately in Fig. S10 of the ESI†). The boiling points at 0.1 MPa (249.1 and 276.7 K; b.p.), melting points at 0.1 MPa (175.5 and 179.5 K; m.p.) and the critical points (c.p. 6.68 MPa/416.3 K and 5.23 MPa/467.2 K) from ref. 27 and 48; the freezing points (f.p.) at 295 K from our DAC experiment; the freezing lines obtained from the m.p. at 0.1 MPa, f.p. at 0.78 GPa/295 K and 0.65 GPa/295 K and from melting points at 1.22 GPa and 1.11 GPa (our optical observations of CH_3Cl and CH_3Br melting in the DAC – spectroscopic pressure calibration and temperature measured by a thermocouple attached to one diamond anvil); diffractometric determinations of CH_3Cl (green circles), CH_3Br phase α (red squares), CH_3Br phase β (red circles), CD_3Br phase α (red square crossed) and CD_3Br phase β (red circle crossed). The red dashed line shows the solid–solid boundary between phases α-CH_3Br and β-CH_3Br. The magnified gas–liquid region is shown in the upper inset: the experimental vapour–pressure data (green and red circles after ref. 27 and 48) and the gas–liquid boundary extrapolation (green and red lines); the enhanced liquid–solid region is shown in the lower inset. Note that the boiling point lines were determined below 0.1 MPa, however, short of reaching the triple points.

The phase diagrams of CH_3Br and CH_3Cl presently outlined in our study are shown in Fig. 1. These phase diagrams of CH_3Cl and CH_3Br have similar melting and boiling boundaries, shifting slightly toward lower temperature and higher pressure for CH_3Cl. In this respect, the transition of CH_3Br between solid phase α, isostructural with the crystal of CH_3I, and phase β, isostructural with CH_3Cl, is particularly intriguing. The crystal structure of perdeutered methyl fluoride, CD_3F, determined by neutron powder diffraction at 5 K, is of the monoclinic space group $P2_1/n$ and is distinctly different from other methyl halides.[30] Presently, we have extended the structural relationship and phase diagrams of CH_3Cl and CH_3Br into the high-pressure region (Fig. 1) and investigated the role of X···X and C–H···X interactions in the CH_3X structures and CH_3Br transformations.

Experimental

Chloromethane, CH_3Cl (m.p. 175.5 K, b.p. 249.1 K), and bromomethane, CH_3Br (m.p. 179.5 K, b.p. 276.7 K), of 99.5% purity from Sigma-Aldrich were used. For high-pressure studies they were loaded into a modified Merrill–Bassett[31] diamond-anvil cell (DAC) by combining compression and cryogenic conditions and *in situ* crystallized. At 295 K, CH_3Cl froze at 0.78 GPa and CH_3Br at 0.65 GPa in the form of a polycrystalline mass, filling the whole volume of the high-pressure chamber. The single crystals of CH_3Cl and CH_3Br (Fig. 2) were obtained under isochoric conditions: the DAC with the polycrystalline mass was heated with a hot-air gun till all but one grain melted. Then the DAC was slowly cooled to room temperature and the single crystal grew and eventually filled the entire volume of the chamber. The experimental details and progress of growing the single crystals of CH_3Cl are shown in Fig. S1–S4† and of CH_3Br in S5–S9 in the ESI.†

Diffraction data were collected at 295 K using a KUMA KM4-CCD diffractometer with graphite-monochromated MoKα radiation.[32] The CrysAlisCCD and CrysAlisRED programs[33] were used for the data collection and determination of the *UB* matrix and for the initial data reduction and *Lp* corrections for both compounds. The intensity of reflections has been accounted for by the absorption of X-rays by the DAC, sample shadowing by the gasket, and absorption of the sample crystal itself.[34,35] The crystal structures of CH_3Cl and CH_3Br were solved by direct methods. H atoms were located from molecular geometry, in α-CH_3Br the disordered model

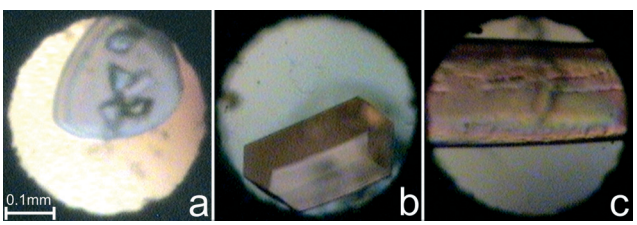

Fig. 2 Single-crystal samples in the diamond-anvil cell: (a) CH_3Cl at 4.38 GPa/483 K; (b) CH_3Br phase α at 1.11 GPa/345 K; and (c) CH_3Br phase β at 1.55 GPa/379 K.

was applied (Shelxl instruction AFIX 137),[36] and the structures were refined with anisotropic C and X atoms. Details of the experiments, structure refinements and crystal data are given in the ESI.†

The program GAUSSIAN03[37] and a PC were used with the B3LYP/3-21G** level of theory for DFT calculations of the electrostatic potential on the surface of CH_3X molecules. Electrostatic potential was mapped onto the molecular surfaces defined as 0.001 a.u. electron-density envelope.[38]

Discussion

Isobaric and isothermal freezing of halomethanes CH_3X leads to the same crystalline phases.[23–25] At 295 K, CH_3Cl and CH_3I crystallize at 0.78 and 0.41 GPa, respectively, in their low-temperature/0.1 MPa phases of CH_3Cl and CH_3I and they are stable within the investigated pressure range. At 295 K, CH_3Br freezes at 0.65 GPa in phase α (space group *Pnma*) and at 1.50 GPa it transforms to phase β (space group $Cmc2_1$). At this transition the unit-cell volume decreases by −4.7 Å^3 (−1.9%) (Fig. 3).

Two main molecular-association types conform to the opposite electrostatic-potential matching principle.[22] In CH_3X molecules the negative electrostatic potential (Fig. 4) is on the rim about the C–X bond, the more positive potential region is on the "caps" of the X atom at the extension of the C–X bond and the highest potential is around the H-atoms. The electrostatic potential magnitude and the area at the extension of C–X bonds increase from F to I (Fig. 4).

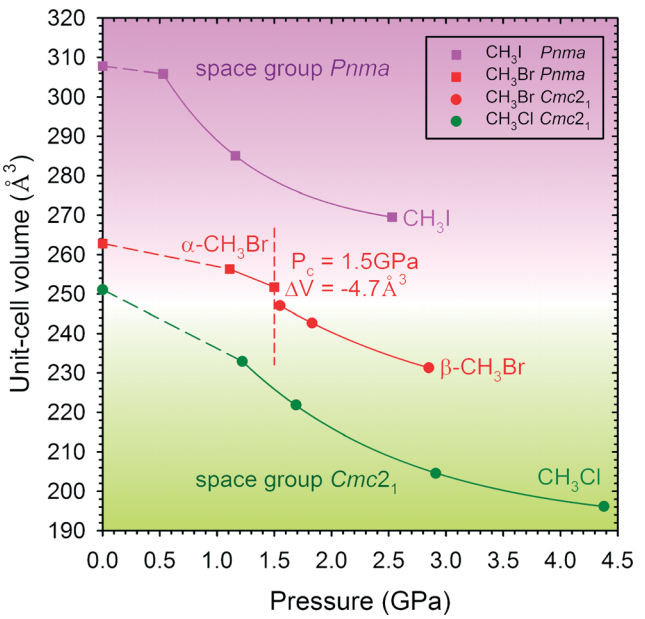

Fig. 3 The molecular volume (unit cell V) as a function of pressure of CH_3Cl (green), CH_3Br (red) and CH_3I (purple). Symmetry $Cmc2_1$ is indicated by circles and *Pnma* by squares. The red dashed vertical line marks the transition between CH_3Br phases α and β. Low temperature/0.1 MPa data from ref. 23–25; 295 K/high pressure data of CH_3I from ref. 26. The dashed lines between the low-temperature/0.1 MPa and 295 K/high-pressure points are for guiding the eye only.

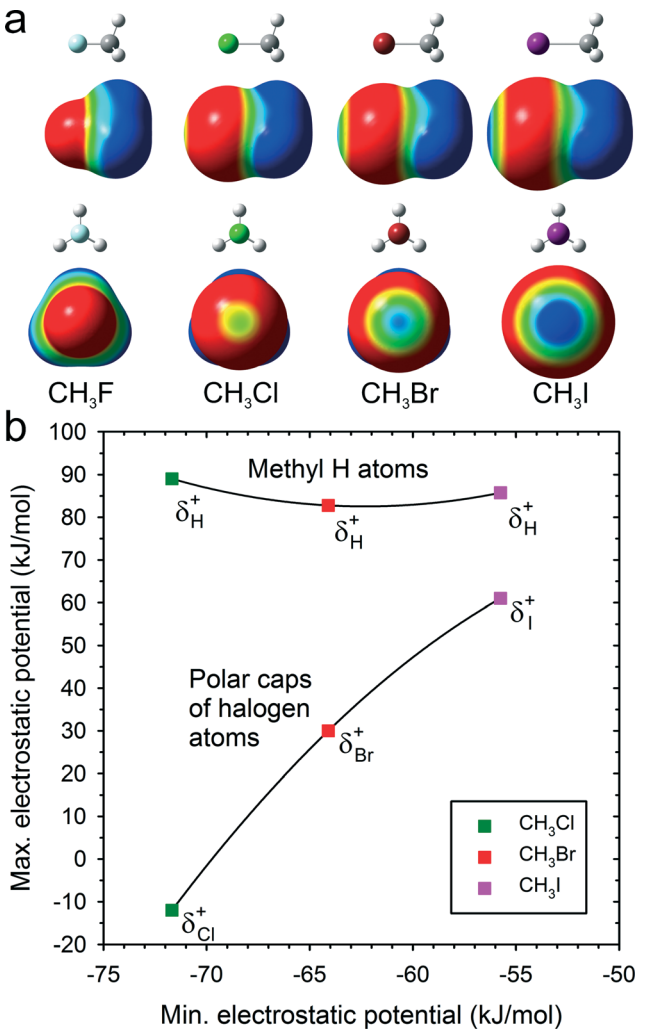

Fig. 4 (a) Molecules CH_3F, CH_3Cl, CH_3Br and CH_3I as well as their surfaces with electrostatic potential colour scale, common for all drawings and ranging from −0.015 (red) to 0.015 a.u. (blue); (b) the electrostatic potential magnitude on the surface of the methyl H-atoms and at the polar caps of the halogens plotted against the minimum potential in all CH_3X surfaces located on the rim of halogen atoms. Symbols δ^+_H and δ^+_X denote the maximum electrostatic potential magnitudes on the surface of H and X atoms, respectively.

Based on the electrostatic-potential magnitudes (Fig. 4), the halogen···halogen interactions in CH_3I are stronger than those in CH_3Br and those in CH_3Cl are still weaker. Indeed, the CH_3I structure is governed by I···I contacts,[26] and no Cl···Cl but C–H···Cl contacts are formed in CH_3Cl.

The positive electrostatic potential on the halogen atom polar region of the molecular surface can act like H-donors in hydrogen bonds. Fig. 4 shows that the magnitude of polar electrostatic potential of the iodine atom is approximately twice as high as that of bromine and that no positive polar potential exists in CH_3Cl. This is consistent with the strongest preference for the X···X bonds in CH_3I and in CH_3Br. The electrostatic potential of the H atoms is higher than that of the I atoms and approximately equal for all CH_3Cl, CH_3Br and CH_3I. A large contribution to the X···X interactions arises

from the polarizability of halogen atoms. This contribution to dispersion forces between Cl···Cl, Br···Br and I···I atoms is equal to −2.5, −3.2 and −4.9 kJ mol^{-1}, respectively. Thus the high positive potential at the polar region of the iodine atom and the strongest dispersion forces of I···I interactions favour the halogen···halogen bonds in CH_3I. The lower positive potential of Br and the weaker dispersion interactions make the Br···Br bonds less competitive. Pressure reverses the balance between the two polymorphs of CH_3Br and it can be argued that it enforces the most efficient involvement of all H-donors in the compressed structure. This pressure effect was observed in sucrose,[16] acetonitrile[14] and formamide.[15]

Halomethanes CH_3X crystallize either in space group $Cmc2_1$ or in space group *Pnma*. Although the space-group symmetries are different, the CH_3X structures have much in common (Fig. 5): the unit cells are roughly similar

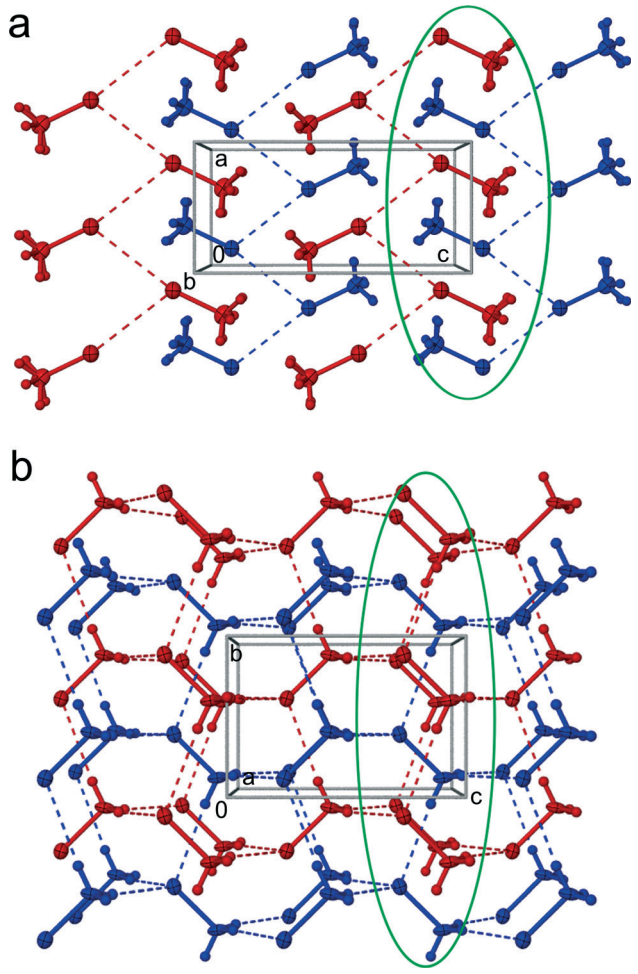

Fig. 5 Two layers of Br···Br bonded CH_3Br molecules in phase α (a) and two interweaved diamondoid C–H···Br bonded networks of phase β (b), shown in autostereographic projections.[49] Dashed lines indicate the shortest intermolecular contacts (*cf.* Table 2). The layers in α-CH_3Br (a) are coloured red (y = 0.75) and blue (y = 0.25); the interpenetrating 3-dimensional networks in β-CH_3Br (b) are discriminated by colours, too. The encircled groups of molecules correspond to the same part of the prototypic Br_2 structure, as explained in the text. The displacement ellipsoids are drawn at the 40% probability level.

Table 1 Selected crystal data of CH_3X (X = Cl, Br, I) phases at their lowest pressure stability region at 295 K

	CH_3I[a]	α-CH_3Br[b]	β-CH_3Br[b]	CH_3Cl[b]
Pressure (GPa)	0.53	1.11	1.55	1.22
Space group	*Pnma*	*Pnma*	$Cmc2_1$	$Cmc2_1$
Unit cell (Å)				
a	4.4968(9)	4.372(5)	6.387(9)	6.314(10)
b	6.8417(14)	6.375(5)	5.163(5)	5.031(9)
c	9.941(2)	9.196(9)	7.492(5)	7.334(9)
Volume (Å^3)	305.83(11)	256.3(4)	247.1(5)	232.9(6)
Z	4	4	4	4

[a] Ref. 26. [b] This work.

(after exchanging axes [*x*] and [*y*]; *cf.* Tables 1 and S1 and S2 in the ESI†), four molecules in the unit cells are located on the mirror planes, and the molecular arrangements in both these symmetries approximate the prototypical orthorhombic symmetry *Cmca* of isostructural Cl_2, Br_2 and I_2 crystals.[39,40] This subgroup–group relationship results from the symmetry of halomethane molecules, C_{3v}, lower than that of the dihalogen molecules, $D_{\infty h}$. Fig. 5 shows that the prototypic *Cmca* symmetry is broken due to the antiparallel arrangement of molecules in α-CH_3Br and the parallel arrangement of molecules in β-CH_3Br. The encircled molecules in the plane perpendicular to [*z*] are all antiparallel in α-CH_3Br (Fig. 5a) and parallel in β-CH_3Br (Fig. 5b). Both these phases correspond to the prototypic Br_2 structure of higher space group symmetry *Cmca*, where the molecules are located on the inversion centres.

In phase α-CH_3Br, of space group symmetry *Pnma*, the molecular layers are linked by Br···Br interactions of type II.[41–43] The positive and negative regions of each bromine atom are electrostatically matched with its two Br neighbours in a zigzag chain (Fig. 5a). The C–Br···Br^i–C^i contacts are asymmetric, with the C–Br···Br angles close to 120° and 170° (see Table 2). Within the layers the electro-positive methyl groups are also arranged in a zigzag motif between the negative rims of the Br atoms in the neighbouring layers (Fig. 5).

In β-CH_3Br the halogen bonds Br···Br are broken and replaced by bonds C–H···Br (Fig. 5b, Table 2). Each CH_3Br molecule forms three C–H···Br bonds on the H-donor side and accepts three C–H···Br bonds around the Br atom. The molecules are arranged head-to-tail into two 3-dimensional interpenetrating (CH···Br)-bonded networks (Fig. 5b). Between these two networks the molecular parts of opposite electrostatic potential are closer than those of the same sign. The difference between phases α and β is most apparent in the ratio of Br···Br contacts contributing 5.5% to the overall Hirschfeld surface at low pressure and this contribution is reduced five-fold at high pressure to about 1%. This rearrangement causes a massive effect for the H···Br Hirschfeld-surface contributions, increasing from 49.6% at 1.11 GPa to 62.1% at 1.55 GPa. These changes in contributing Hirschfeld areas are compensated for in the reduced surface of H···H contacts of 44.9% and 36.9%, respectively.

Table 2 Selected interatomic distances (Å) and angles (°) of the crystalline CH_3Br phase α and β structure at high pressure compared with those observed at low-temperature. Intermolecular distances shorter than the sum of van der Waals radii[52] are written in bold

	Phase α	Phase α	Phase α
CH_3Br at:	0.1 MPa/153 K[a]	1.11 GPa/295 K[b]	1.50 GPa/295 K[b]
Molecular dimensions			
C1–Br1 (Å)	1.863	1.912(10)	1.898(9)
Intermolecular dimensions			
Br1···Br1^{i} (Å)	**3.587**	**3.571(3)**	**3.546(3)**
∠C1–Br1···Br1^{i} (°)	116.0	118.5(4)	116.5(2)
∠Br1···Br1^{i}–C1^{i} (°)	166.8	166.0(4)	168.2(2)
C1···Br1^{j} (Å)	3.882	3.825(8)	3.844(4)
H12···Br1^{k} (Å)	3.124	3.242	3.058
H11···Br1^{l} (Å)	3.170	3.315	3.084
	Phase β	Phase β	Phase β
CH_3Br at:	1.55 GPa/295 K[b]	1.83 GPa/295 K[b]	2.85 GPa/295 K[b]
Molecular dimensions			
C1–Br1 (Å)	1.919(16)	1.892(14)	2.024(25)
Intermolecular dimensions			
Br1···Br1^{m} (Å)	3.948(3)	3.908(4)	3.878(9)
∠C1–Br1···Br1^{m} (°)	63.9(5)	62.6(5)	62.4(7)
∠Br1···Br1^{m}–C1^{m} (°)	152.9(5)	154.3(5)	152.7(7)
C1···Br1^{n} (Å)	**3.501(16)**	**3.487(15)**	**3.313(24)**
C1···Br1^{o} (Å)	3.551(17)	**3.471(18)**	**3.444(24)**
C1···Br1^{p} (Å)	3.671(9)	3.684(9)	3.599(14)
H1···Br1^{q} (Å)	3.073	3.094	**2.909**
H3···Br1^{r} (Å)	**3.041**	**3.009**	**2.897**

[a] Ref. 24. [b] This work. Symmetry codes: (i) 0.5 + *x*, 0.5 − *y*, 0.5 − *z*; −0.5 + *x*, 0.5 − *y*, 0.5 − *z*; (j) −*x*, −0.5 + *y*, −*z*; −*x*, 0.5 + *y*, −*z*; (k) 1 − *x*, 0.5 + *y*, −*z*; (l) 1 − *x*, −0.5 + *y*, −*z*; (m) −*x*, −*y*, 0.5 + *z*; −*x*, −*y*, −0.5 + *z*; (n) −*x*, 1 − *y*, 0.5 + *z*; (o) −*x*, −*y*, 0.5 + *z*; (p) −0.5 + *x*, 0.5 + *y*, *z*; 0.5 + *x*, 0.5 + *y*, *z*; (q) *x*, 1 + *y*, *z*; (r) −0.5 − *x*, 0.5 − *y*, 0.5 + *z*; 0.5 − *x*, 0.5 − *y*, 0.5 + *z*.

Isobaric,[25] isothermal and isochoric crystallization of CH_3Cl all lead to the same phase isostructural with β-CH_3Br. It is apparent that weaker Cl···Cl interactions are overcome by C–H···Cl bonds (see Table 3) and no *Pnma*-symmetric polymorph is formed. The CH_3Cl structure is consistent with the chlorophobic rule.[44,45]

It is remarkable that CH_3Br phase β is isostructural with the high-pressure acetonitrile phase β.[14] The CH_3Br and CH_3CN molecules are similar in shape and in the electrostatic potential distribution on the molecular surface (except the polar Br-atom positive region, which is not involved in the C–H···Br bonds). Also, the favoured directions of C–H···X bonds are similar. Consequently, a similar aggregation of three molecules around each –Br and ≡N atoms takes place (Fig. 6). The difference, that in acetonitrile the transition is induced by the transformation between 2-fold C–H···N (α-CH_3CN) to 3-fold C–H···N (β-CH_3CN) bonding whereas methyl bromide transforms between 2-fold Br···Br (α-CH_3Br) to 3-fold C–H···Br

Table 3 Selected interatomic distances (Å) and angles (°) of the crystalline CH_3Cl structure at high pressure compared with those observed at low temperature. Intermolecular distances shorter than the sum of van der Waals radii[52] are distinguished in bold

CH_3Cl at:	0.1 MPa/148 K[a]	1.22 GPa/295 K[b]	1.69 GPa/295 K[b]	2.91 GPa/295 K[b]	4.38 GPa/295 K[b]
Molecular dimensions					
C1–Cl1 (Å)	1.805	1.746(7)	1.792(4)	1.750(5)	1.716(7)
Intermolecular dimensions					
Cl1···Cl1^{i} (Å)	4.010	3.906(5)	3.871(8)	3.712(5)	3.670(7)
∠C1–Cl1···Cl1^{i} (°)	64.4	63.4(3)	61.7(2)	66.3(2)	64.7(3)
∠Cl1···Cl1^{i}–C1^{i} (°)	156.1	156.9(3)	156.5(1)	151.0(2)	151.1(2)
C1···Cl1^{j} (Å)	3.507	3.454(8)	**3.371(5)**	**3.316(6)**	**3.285(8)**
C1···Cl1^{k} (Å)	3.618	3.493(9)	**3.407(5)**	**3.409(7)**	**3.322(8)**
C1···Cl1^{l} (Å)	3.734	3.650(6)	3.582(5)	**3.421(3)**	**3.391(8)**
H1···Cl1^{m} (Å)	3.138	3.085	2.962	**2.788**	**2.706**
H3···Cl1^{n} (Å)	3.125	3.011	**2.926**	**2.855**	**2.823**

[a] Ref. 25. [b] This work. Symmetry codes: (i) −*x*, −*y*, 0.5 + *z*; −*x*, −*y*, −0.5 + *z*; (j) −*x*, 1 − *y*, 0.5 + *z*; (k) −*x*, −*y*, 0.5 + *z*; (l) −0.5 + *x*, 0.5 + *y*, *z*; 0.5 + *x*, 0.5 + *y*, *z*; (m) *x*, 1 + *y*, *z*; (n) −0.5 − *x*, 0.5 − *y*, 0.5 + *z*; 0.5 − *x*, 0.5 − *y*, 0.5 + *z*.

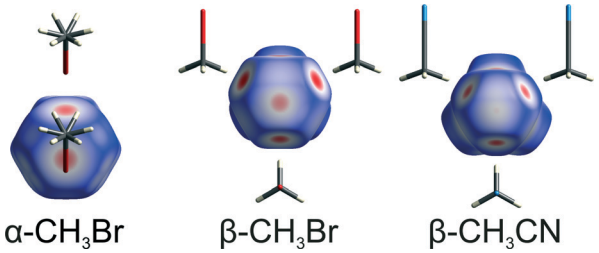

Fig. 6 Hirschfeld surfaces[50,51] of α-CH_3Br, β-CH_3Br and β-CH_3CN[14] viewed along the molecular axis from the Br/N-top of molecules and decorated with colour maps of intermolecular distances relative to the van der Waals radii. Other interacting molecules are shown as stick models. Distances longer than van der Waals radii are shown in shades of navy blue, the equal ones are white and the shorter red. The colour scale ranges from −0.15 to 0.65.

(β-CH_3Br) bonding, is meaningful. It indicates that, apart from other factors, the steric hindrance between large halogen atoms can be disadvantageous for their close association.

Conclusions

Phase α-CH_3Br, isostructural with CH_3I and dominated by halogen···halogen bonds, is destabilized by pressure and transforms into phase β-CH_3Br governed by C–H···halogen interactions. Phase β of CH_3Br and the CH_3Cl crystal are isostructural. It can be envisaged that CH_3I may also transform into a C–H···I bonded phase at pressure considerably higher than 2.5 GPa as obtained in our previous study.[26] Due to halogen···halogen and C–H···halogen forces systematically increasing in the $CH_3Cl < CH_3Br < CH_3I$ sequence, only CH_3Cl up to 1.2 GPa and CD_3Br phase β determined at ambient pressure and 175 K[29] are the loose crystals.[46,47] This indicates that CH_3X molecules are more evenly accommodated in space group $Cmc2_1$ and that C–H···X interactions are favoured by the close-packing effect. This effect can significantly contribute to the stability of CH_3X at high pressure. However, detailed measurements of the CH_3Br crystal volume as a function of temperature are still needed to evaluate the contribution of close packing to the C–H···X *versus* X···X competition.

Acknowledgements

This study was supported by the TEAM grant no. 2009-4/6 from the Foundation for Polish Science.

Notes and references

1 F. F. Awwadi, R. D. Willett, K. A. Peterson and B. Twamley, *Chem. – Eur. J.*, 2006, **12**, 8952–8960.
2 C. M. Reddy, M. T. Kirchner, R. V. Gundakaram, K. A. Padmanabhan and G. R. Desiraju, *Chem. – Eur. J.*, 2006, **12**, 2222–2234.
3 P. Metrangolo, F. Meyer, T. Pilati, G. Resnati and G. Terraneo, *Angew. Chem., Int. Ed.*, 2008, **47**, 6114–6127.
4 A. Mukherjee and G. R. Desiraju, *IUCrJ*, 2014, **1**, 49–60.
5 P. Politzer, J. S. Murray and T. Clark, *Phys. Chem. Chem. Phys.*, 2013, **15**, 11178–11189.
6 A. R. Jagarlapudi, P. Sarma and G. R. Desiraju, *Acc. Chem. Res.*, 1986, **19**, 222–228.
7 P. Metrangolo and G. Resnati, *Science*, 2008, **321**, 918–919.
8 T. J. Mooibroek and P. Gamez, *CrystEngComm*, 2013, **15**, 4565–4570.
9 S. L. Price, A. J. Stone, J. Lucas, R. S. Rowland and A. E. Thornley, *J. Am. Chem. Soc.*, 1994, **116**, 4910–4918.
10 M. Kaźmierczak and A. Katrusiak, *Cryst. Growth Des.*, 2014, **14**, 2223–2229.
11 H.-C. Chang, J.-C. Jiang, C.-W. Chuang and S. H. Lin, *Chem. Phys. Lett.*, 2004, **397**, 205–210.
12 K. F. Dziubek, D. Jęczmiński and A. Katrusiak, *J. Phys. Chem. Lett.*, 2010, **1**, 844–849.
13 K. M. Lee, H.-C. Chang, J.-C. Jiang, J. C. C. Chen, H.-E. Kao, S. H. Lin and I. J. B. Lin, *J. Am. Chem. Soc.*, 2003, **125**, 12358–12364.
14 A. Olejniczak and A. Katrusiak, *J. Phys. Chem. B*, 2008, **112**, 7183–7190.
15 R. Gajda and A. Katrusiak, *Cryst. Growth Des.*, 2011, **11**, 4768–4774.
16 E. Patyk, J. Skumiel, M. Podsiadło and A. Katrusiak, *Angew. Chem., Int. Ed.*, 2012, **51**, 2146–2150.
17 M. Podsiadło, K. Dziubek and A. Katrusiak, *Acta Crystallogr., Sect. B: Struct. Sci.*, 2005, **61**, 595–600.
18 M. Podsiadło, K. Dziubek, M. Szafrański and A. Katrusiak, *Acta Crystallogr., Sect. B: Struct. Sci.*, 2006, **62**, 1090–1098.
19 M. Podsiadło and A. Katrusiak, *Acta Crystallogr., Sect. B: Struct. Sci.*, 2007, **63**, 903–911.
20 M. Podsiadło and A. Katrusiak, *J. Phys. Chem. B*, 2008, **112**, 5355–5362.
21 M. Podsiadło and A. Katrusiak, *CrystEngComm*, 2008, **10**, 1436–1442.
22 M. Podsiadło and A. Katrusiak, *CrystEngComm*, 2009, **11**, 1391–1395.
23 R. M. Ibberson and M. Prager, *Z. Kristallogr.*, 2007, **222**, 416–419.
24 T. Kawaguchi, M. Hijikigawa, Y. Hayafuji, M. Ikeda, R. Fukushima and Y. Tomiie, *Bull. Chem. Soc. Jpn.*, 1973, **46**, 53–56.
25 R. D. Burbank, *J. Am. Chem. Soc.*, 1953, **75**, 1211–1214.
26 M. Podsiadło and A. Katrusiak, *CrystEngComm*, 2009, **11**, 1951–1957.
27 C. J. Egan and J. D. Kemp, *J. Am. Chem. Soc.*, 1938, **60**, 2097–2101.
28 O. S. Binbrek, A. Anderson and B. H. Torrie, *J. Chem. Phys.*, 1985, **82**, 1468–1475.
29 P. N. Gerlach, B. H. Torrie and B. M. Powell, *Mol. Phys.*, 1986, **57**, 919–930.
30 R. M. Ibberson and M. Prager, *Acta Crystallogr., Sect. B: Struct. Sci.*, 1996, **52**, 892–895.
31 W. A. Bassett, *High Pressure Res.*, 2009, **29**, 163–186.
32 A. Budzianowski and A. Katrusiak, *High-Pressure Crystallography*, ed. A. Katrusiak and P. F. McMillan, Kluwer Academic Publisher, Dordrecht, 2004, pp. 101–112.

33 Oxford Diffraction Ltd., *Xcalibur CCD system, CrysAlis Software system, Version 1.171*, 2004.
34 A. Katrusiak, *REDSHABS – Program for Correcting Reflections Intensities for DAC Absorption, Gasket Shadowing and Sample Crystal Absorption*, Adam Mickiewicz University, Poznań, Poland, 2003.
35 A. Katrusiak, *Z. Kristallogr.*, 2004, **219**, 461–467.
36 G. M. Sheldrick, *Acta Crystallogr., Sect. A: Found. Crystallogr.*, 2008, **64**, 112–122.
37 M. J. Frisch, *et al.*, *GAUSSIAN03, Revision B.04.*, Gaussian, Inc., Pittsburgh, PA, USA, 2003.
38 R. F. W. Bader, M. T. Carroll, J. R. Cheeseman and C. Chang, *J. Am. Chem. Soc.*, 1987, **109**, 7968–7979.
39 R. M. Ibberson, O. Moze and C. Petrillo, *Mol. Phys.*, 1992, **76**, 395–403.
40 B. M. Powell, K. M. Heal and B. H. Torrie, *Mol. Phys.*, 1984, **53**, 929–939.
41 G. R. Desiraju and R. Parthasarathy, *J. Am. Chem. Soc.*, 1989, **111**, 8725–8726.
42 P. Metrangolo and G. Resnati, *IUCrJ*, 2014, **1**, 5–7.
43 T. Sakurai, M. Sundaralingam and G. A. Jeffrey, *Acta Crystallogr.*, 1963, **16**, 354–363.
44 O. V. Grineva and P. M. Zorky, *Zh. Fiz. Khim.*, 1998, **72**, 714–720 (In Russian).
45 O. V. Grineva and P. M. Zorky, *Kristallografiya*, 2000, **45**, 692–698 (In Russian).
46 M. Bujak, M. Podsiadło and A. Katrusiak, *CrystEngComm*, 2011, **13**, 396–398.
47 M. Kaźmierczak and A. Katrusiak, *J. Phys. Chem. C*, 2013, **117**, 1441–1446.
48 D. R. Lide, *CRC Handbook of Chemistry and Physics*, CRC Press Inc., Boca Raton, FL, 90th edn, 2010.
49 A. Katrusiak, *J. Mol. Graphics Modell.*, 2001, **19**, 363–367.
50 J. J. McKinnon, M. A. Spackman and A. S. Mitchell, *Acta Crystallogr., Sect. B: Struct. Sci.*, 2004, **60**, 627–668.
51 S. K. Wolff, D. J. Grimwood, J. J. McKinnon, D. Jayatilaka and N. A. Spackman, *CrystalExplorer 2.0*, University of Western Australia, Perth, Australia, 2007.
52 A. Bondi, *J. Phys. Chem.*, 1964, **68**, 441–451.